pISSN 1229-3008 eISSN 2287-6251
Progress in Superconductivity and Cryogenics
Vol.22, No.3, (2020), pp.1~6 https://doi.org/10.9714/psac.2020.22.3.001

Performance analysis of a 746 W HTS generator equipped with 70 A class contactless superconducting field exciter

Yoon Seok Chae, and Ho Min Kim*

Department of Electrical Engineering, Jeju National University, Jeju,63243, Korea

(Received 24 August 2020; revised or reviewed 28 September 2020; accepted 29 September 2020)

Abstract

This paper presents the analysis results on the electrical output performance characteristics of a 746 W high temperature superconducting generator (HTSG). The HTS field winding is charged by non-contact excitation method, i.e., contactless superconducting field exciter (CSFE) which is originated by rotary flux pump based on permanent magnet. In this paper, the preliminary current charging test was carried out using a 70 A CSFE to evaluate the performance of field exciter and analyze its non-contact excitation characteristics for the full-scale HTS field winding of the 746 W HTSG. First, the various contactless current-charging tests were conducted using assembly with HTS field winding and CSFE. Then, in order to estimate the output power performance characteristics of the 746 W HTSG, finite element analysis was conducted based on field excitation information which is experimentally measured under various operating conditions. Finally, the electrical output characteristics in no-load and load models were simulated by two-dimensional transient solver in ANSYS electromagnetics 19.0 release.

Keywords: contactless superconducting field exciter, finite element analysis, high temperature superconducting generator, high temperature superconducting field winding

1. INTRODUCTION

This paper presents the electrical characteristic analysis of a 746 W HTSG using CSFE, which is originated from permanent magnet based on HTS flux pump, and is a excitation method to charge direct current (DC) to HTS coil in a non-contact manner [1–13].

In this system, by integrating the CSFE into the rotor of HTSG, DC power is generated by itself and injected into the HTS field winding in a non-contact manner; thus, it is possible to eliminate the external DC power source, slip ring/brush assembly, and current leads which are constituting the conventional contact excitation system, thereby resulting in improvement in system efficiency and in electrical/thermal stabilities of HTS field winding, as well as in saving in cooling cost due to the reduction of cryogenic cooling load. Moreover, it has advantage in terms of reducing the maintenance cost by simplifying the structural configuration due to removal of the power slip ring /brush assembly.

In this paper, a 70 A class CSFE was fabricated and the charging performance and operating characteristics of the field current (I_f) were experimentally analyzed in preliminary tests. In particular, to confirm the technical feasibility of this contactless excitation method i.e., a CSFE, on application to the 746 W HTSG, the HTS field winding were excited under various charging frequency (f_r) of CSFE in a stationary flux-pump mode before the final fabrication and assembly of HTSG.

Next, the electrical output characteristics of HTS were analyzed using the non-contact charging results in the preliminary tests as the input parameters for HTS field winding to assure and estimate the output power performance characteristics of the 746 W HTSG. For the non-loaded and loaded operations in the generator mode, the two-dimensional finite element analysis (2-D FEA) was performed using ANSYS Electromagnetics Suite 19.0 release.

* Corresponding author: hmkim@jejunu.ac.kr

2. CONTACTLESS CURRENT CHARGE TESTS

2.1. Current charge characteristics of CSFE

The operational mechanism of the 2G HTS flux pump excitation device based on rotating permanent magnets (PMs), which is applied as CSFE in this paper, can be described by DC open-circuit voltage (V_{dc}) and dynamic resistance (R_d) connected in series with the superconducting loop. Figs. 1 and 2 show the conceptual schematic diagram that consist of HTS load magnet and rotary-type 2G HTS flux pump, and its corresponding equivalent circuit to explain the fundamental principle of current charge by the 2G HTS flux pump, respectively. In general, flux pump device consists of a 2G HTS wire in the stator and several PMs that are arranged on the circumference of the rotor. Moreover, this flux pump is electrically connected with superconducting magnets to be charged and then, it forms a closed electrical circuit in a superconducting state. At this time, when the PMs rotate with constant rotating speed (N_s), the time-varying magnetic field with constant (f_r) is injected into 2G HTS wire of the stator. Consequently, a partially rectified DC power source is generated by itself, and thus the current can be charged in a non-contact manner to the

superconducting magnets [11, 14–16].

The current charge/discharge characteristic can be expressed by an electrical R-L circuit with a relatively very large time constant (τ), as shown in Fig. 2, and is governed as follows [4, 13, 16]:

$$V_{dc} = L_c \frac{dI_t}{dt} + I_t R_e \tag{1}$$

where V_{dc} is equivalent DC power source which is induced to 2G HTS flux pump and Lc denotes the inductance of the HTS magnet for electric load. R_e is total resistance in the superconducting loop and sum of the dynamic resistance (R_d) and joint resistance by soldering (R_j), i.e., $R_e = R_d + R_j$. Especially, R_{j1} and R_{j2} are joint resistance between CSFE and HTS magnet. DC transport current (I_t) that flows through the circuit and terminal voltage of HTS magnet (V_m), which are exponentially dependent on the elapsed time, are given as follows [4, 8, 12, 13, 17]:

$$I_t(t) = \frac{V_{dc}}{R_e}\left(1 - e^{-\frac{R_e}{L_c}t}\right) = I_{sc}\left(1 - e^{-\frac{R_e}{L_c}t}\right) \tag{2}$$

$$V_{coil}(t) = L_c \frac{dI_t}{dt} = V_{dc} \cdot e^{-\frac{R_e}{L_c}t} \tag{3}$$

where L_c/R_e denotes the τ and determines the charge time of the ramped-up I_t. I_{sc} is defined as the function of V_{dc}/R_e, which is the maximum available current that can be transferred into the loaded HTS magnet by flux pump.

Fig. 3 shows the correlation of the major parameters contributing to the operational characteristics and performance of flux pump excitation device. It focuses on relatively high I_s and fast charging time (t_e) as the key parameters for design and control on the operational characteristics of HTS flux pump. For maximizing I_s, first, high V_{dc}, which is achieved by increasing the linkage flux (Φ_l) and fast f_r, which is the applied speed of Φ_l, are considered. Moreover, for minimizing the t_e, the high R_d and low L_c are considered, and this can be achieved by increasing f_r and decreasing the number of turns in coil (N_c), respectively. These parameters are critically effective for decision on $\downarrow\tau$ ($=\downarrow L_c/\downarrow R_e$) of the superconducting circuit. Here, R_j is constant; thus, the R_e is dependent only on R_d during operation.

2.2. Current charge tests of full-scale HTS field winding

Since the R_j at both ends of R-L circuit and L_c of HTS load magnet are constant, τ and I_s are determined by R_d based on the equivalent circuit model, as mentioned in section 2.1. Thus, f_r is generally considered as very important parameter in the operational performance and characteristic of CSFE because R_d is linearly proportional to the f_r in a specific speed section [18 – 21].

Fig. 4 shows the three-dimensional configuration of full-scale HTS field winding assembled with CSFE. The 2G HTS wires with 12 mm width from SuperPower Inc. (SC12050 model) were wound on four-salient field poles

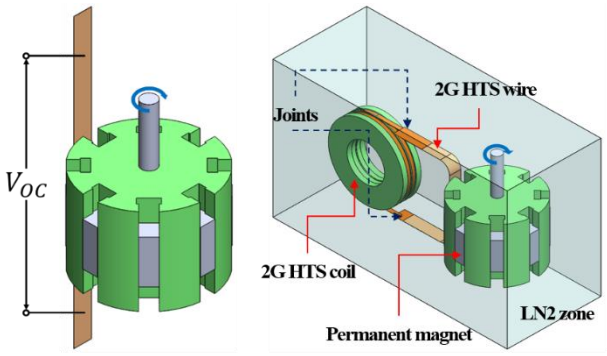

Fig. 1. Conceptual configuration of 2G HTS flux pump based on rotating magnet.

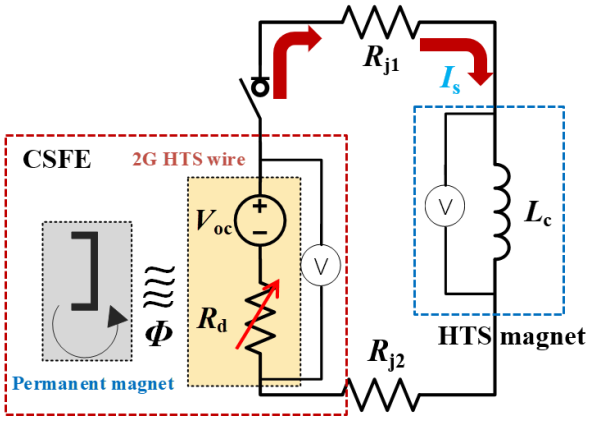

Fig. 2. Equivalent superconducting R-L circuit between flux pump excitation device and HTS load magnet.

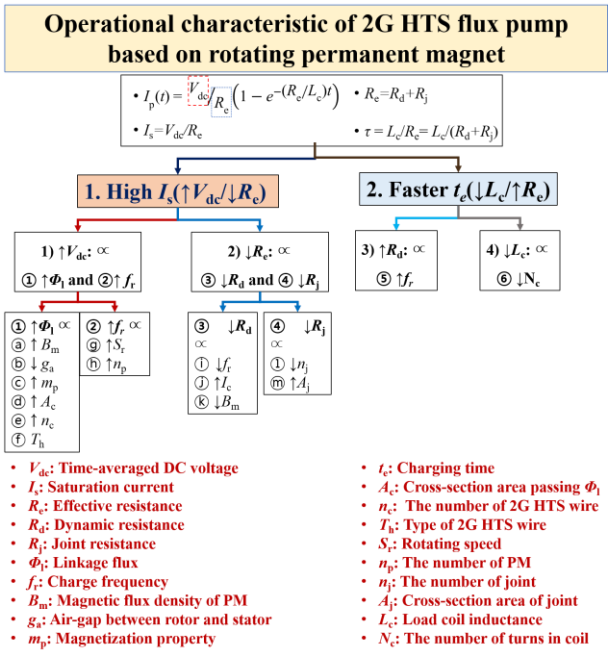

Fig. 3. Operational characteristics of 2G HTS flux pump based on rotating magnet.

with single racetrack formation. The averaged value of I_c for four-HTS field winding was measured to be 128 A at 77 K and self-field. The 2G HTS wires with 12.1 mm width from SuNAM Co., Ltd (SCN12550 model) were wound in

series on aluminum toroidal head of CSFE rotor and their two ends were mechanically jointed with two ends of HTS field winding using In-Bi soldering to create the electrically-closed circuit. The T-shaped neodymium magnets with a surface center magnetic flux density of 0.52 T (N50) were used for CSFE stator [22 – 24].

Fig. 5 shows experimental setup for current charge tests. In the tests, the CSFE stator, where the N50 PMs were installed, was the only rotating part for simplicity of the test environment. A servomotor operated and controlled this rotating part and its N_s (or f_r). However, CSFE's stator is stationary in real-operation of HTSG. The assembly between CSFE and HTS field winding was finally inserted into the cylindrical SUS cryostat to cool down by liquid nitrogen bath. The magnetic field density of the PM for the N50 grade was measured to be approximately 0.15 T at LN2 temperature, i.e., 77 K, and air-gap of 7 mm which is defined to geometric distance between the rotor and stator of CSFE [23].

In this experiment, the number of PMs (n_p) in the CSFE stator was considered to control the f_r (= $n_p \times N_s$)/60) of CSFE. Thus, we changed the n_p from 4 to 16 with N_s under 200 rpm to investigate the operational characteristic and performance of I_s charged by CSFE according to changes in the f_r. Figs. 6 and 7 show the experimental results of the current charge tests according to the changes in n_p from 4 to 16 with different values of N_s (100, 150, and 200 rpm). Generally, the magnitude and charge speed of I_s are enhanced with an increase in f_r, as mentioned in section 2.1. The chargeable current ranges for full-scale HTS field winding were approximately from 49.5 to 70.4 A at f_r values from 6.7 to 53.3 Hz. Moreover, the charging time (t_e) was calculated based on the time constant during the circuit charge, which means the elapsed time reaching 63.2% of I_s, and they were compared in Table I. It was observed that t_e was generally accelerated with increasing f_r. Finally, it concluded that to control the I_s values below 49.6 A, the magnetic flux linked to 2G HTS wires of the CSFE rotor should be decreased by controlling air-gap length in this system [23].

The excitation loss of developed CSFE was compared with that of metal current lead pairs in contact excitation system. If HTS field winding was excited with current of 70.4 A by the contact excitation system, the excitation losses in copper- and brass-current lead pairs with round

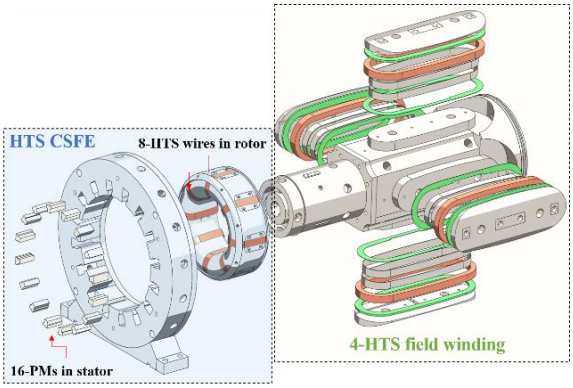

Fig. 4. Three-dimensional configuration of full-scale HTS field winding assembled with CSFE.

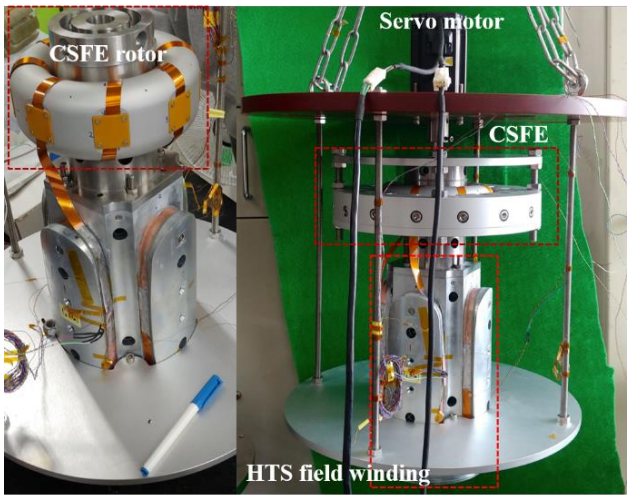

Fig. 5. Experimental setup of non-contact current charge tests for HTS field winding of 746 W HTSG.

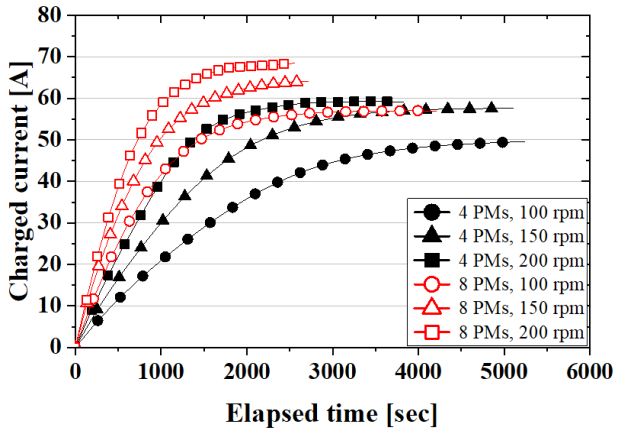

Fig. 6. I_s curves according to changes in n_p (= 4 and 8) and N_s (= 100, 150, and 200 rpm).

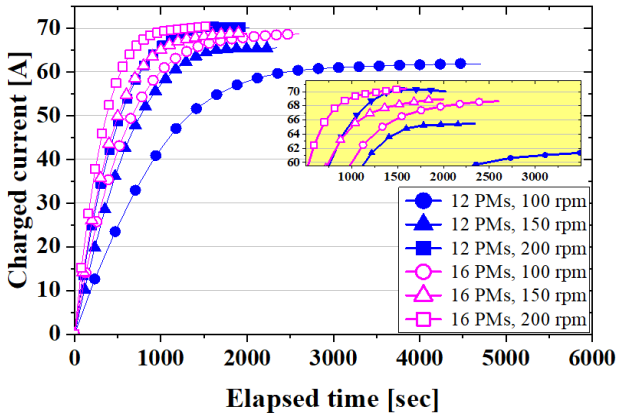

Fig. 7. I_s curves according to changes in n_p (= 12 and 16) and N_s (= 100, 150, and 200 rpm).

rods were estimated to be 11.94 W (= 5.97 W × 2 pairs) and 8.98 W (= 4.49 W × 2 pairs), respectively, as shown in Fig. 8. Here, we calculated the minimum lead diameters of 3.4 and 7.8 mm in case of copper and brass materials, respectively, with an assumption of 330 mm axial length, which is considered by structural distance between end at

300 K and end at 77 K of round rod-type lead. Moreover, we considered averaged electrical resistivity (ρ) and thermal conductivity (k) from 300 K to 77 K (ρ_{copper} = 460 W/mK and k_{copper} = 17.5 nΩ) and (ρ_{brass} = 65 W/mK and k_{brass} = 70 nΩ) [25 – 26]. However, if the HTS field winding was charged by the CSFE, the excitation loss was estimated to be 0.54 W, with an assumption of R_e of 0.1086 mΩ. It is observed that the values of R_e (=L_c/τ) can be roughly calculated with I_s test result of 70.4 A charge case, as shown in Fig. 7. In an equal operating condition, the 70 A class CSFE is possible to reduce the excitation loss by approximately 95.5% and 94%, respectively, as compared to that of the copper- and brass-current leads in conventional contact excitation system [24].

TABLE I
CHARGING TEST RESULTS ACCORDING TO THE CHANGES IN F_R.

Test cases	Charging time†/current# [s]/[A]	Max. charge current [A]
4 PMs at 100 rpm (6.7 Hz)	1660/31.3	49.5
4 PMs at 150 rpm (10 Hz)	1280/36.5	57.7
4 PMs at 200 rpm (13.3 Hz)	922/37.5	59.3
8 PMs at 100 rpm (13.3 Hz)	795/36.1	57
8 PMs at 150 rpm (20 Hz)	690/40.5	64.1
8 PMs at 200 rpm (26.7 Hz)	582/43.3	68.4
12 PMs at 100 rpm (20 Hz)	886/39.2	62
12 PMs at 150 rpm (30 Hz)	564/41.4	65.5
12 PMs at 200 rpm (40 Hz)	439/44.5	70.4
16 PMs at 100 rpm (26.7Hz)	524/43.4	68.6
16 PMs at 150 rpm (40 Hz)	400/43.6	68.9
16 PMs at 200 rpm (53.3 Hz)	304/44.5	70.4

†: Charging time to reach 0.632I_s, #: 0.632I_s

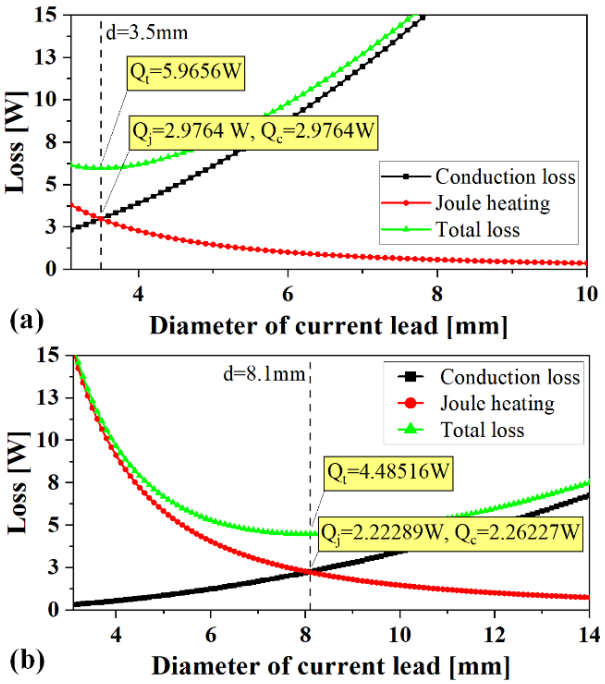

Fig. 8. Variations in heat loss versus diameters of the (a) copper- and (b) brass-current lead.

TABLE II
DESIGN PARAMETER SPECIFICATIONS OF THE 746 W HTSG.

Parameters	Unit	Value
Rated power	W	746
Rated rotating speed	rpm	400
Rotor pole number	-	4
Number of slots	-	48
Stator coil number per slot/phase	-	52/416
Fill factor of stator slot	%	58
Magnetic air-gap	mm	7
Mechanical air-gap	mm	1
Operating field winding current	A	≥40
Critical current of field winding	A	127.5
Total inductance of field winding	mH	32.9
Total turns of field winding	-	240
HTS coil type	-	Race-track DPC
Winding type	-	Polyimide tape insulation
Operating temperature	K	77
Cooling method	-	LN_2 batch

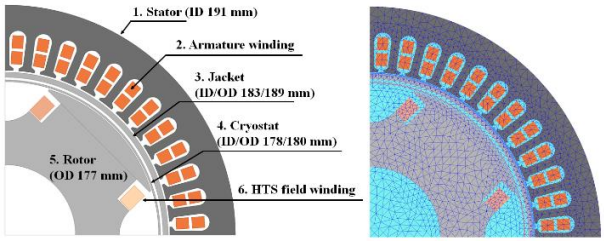

Fig. 9. 2-D FEA model and mesh plot.

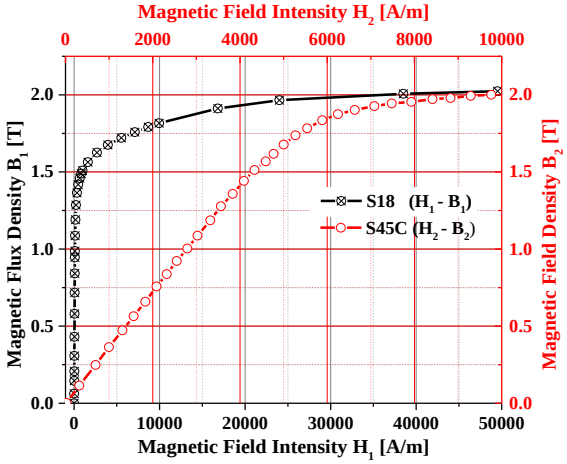

Fig. 10. *B–H* characteristic curves for stator core (S18) and rotor core (S45C).

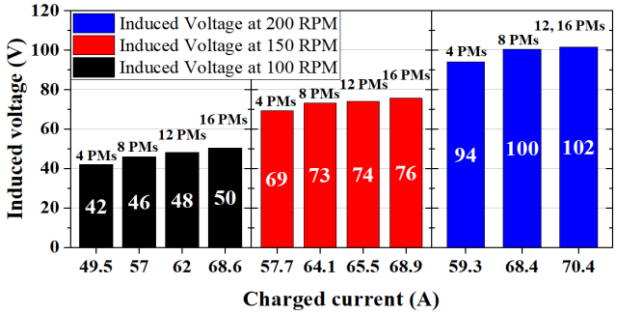

Fig. 11. E_i comparison in armature open circuit of the 746 W HTSG at N_s of 100, 150, and 200 rpm.

3. OUTPUT CHARACTERISTIC ANALYSIS

Table II lists the design parameter specifications of a 746 W HTSG to build 2-D FE models as shown in Fig. 9. The carbon steel (SAE-AISI 1045 or S45C) and laminated thin steel plates (50PN470 or S18) were used as the material for the iron cores in rotor and stator, respectively. Fig. 10 shows the magnetic field density (B) versus intensity (H) characteristic curves of the stator and rotor cores, which are referred from [27 – 28].

For non-loaded and loaded operations in the generator mode, the time-step 2-D FEA in ANSYS Electromagnetics Suite 19.0 release was carried out using approximately 5692 finite elements, as shown in Fig. 9. Fig. 11 shows the open circuit curves of the 746 W HTSG at the various N_s using I_f information based on non-contact current charge tests in Table 1. It shows the induced voltage (E_i) in the armature winding according to each N_s corresponding to excited I_f by CSFE. Based on Faraday's law, the E_i in the armature winding is proportional to the main magnetic field from field winding which is linked with the armature winding and its N_s. Thus, the high N_s and the large n_p in the CSFE stator exhibited the larger E_i in the armature winding, as shown in Fig. 11 because the I_f, which increases main magnetic field, is proportional to the n_p.

When comparing the n_p of 12 and 16 at 200 rpm, the values of charged I_f are practically the same as 70.4 A even though the Φ_l in CSFE increased according to an increase of n_p in CSFE stator; thus, the magnitudes of the E_i are also the same. The generated ranges of E_i were calculated from 93.9 to 101.56 V_{rms} at the rated rotating speed of 200 rpm.

Fig. 12 shows the 2-D magnetic field distributions for the 746 W HTSG in open circuit condition. As analysis result, it was confirmed that the magnetic cores in rotor and stator start to saturate within the controllable ranges of the I_f in this CSFE. Together, the values of E_i start to saturate as shown in Fig. 10.

Fig. 13 shows the analysis results in constant load of the 746 W HTSG according to changes in n_p (I_f) and N_s. A constant resistive load of 30 ohm was electrically connected with 2-D FE model. As analysis result, it was confirmed that the output powers of over 746 W, which is the rated capacity of this machine, were generated above the f_r values of 13.3 (4 PMs, 200 rpm), 26.7 (8 PMs, 200 rpm), 40 (12 PMs, 200 rpm), and 53.3 (16 PMs, 200 rpm) Hz. In conclusion, the I_f values of over 60 A are required to achieve the rated design of this machine through proper excitation combinations with n_p and N_s.

Figs. 14 and 15 show the constant speed curves of the 746 W HTSG with the I_f of 49.5 A and the N_s of 100 rpm and the I_f of 70.4 A and the N_s of 200 rpm, respectively, according to changes in load resistance. In case of field excitation with the I_f of 49.5 A (f_r = 6.7 Hz), it was not possible to generate the target capacity of this HTSG. In case of field excitation with the I_f of 70.4 A (f_r = 40 and 53.3 Hz), the rated output power of 955 W was generated with terminal voltage of 175.8 V_{rms} and armature current of 3.1 A_{rms}.

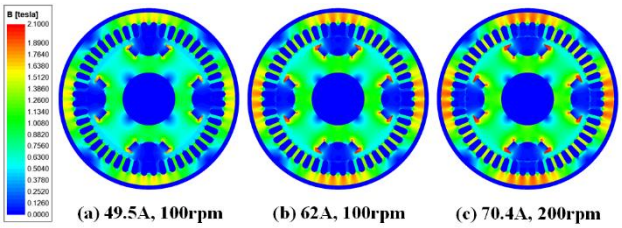

Fig. 12. 2-D magnetic field distributions at I_f charges of (a) 49.5, (b) 62, (c) 70.4 A in open circuit analysis.

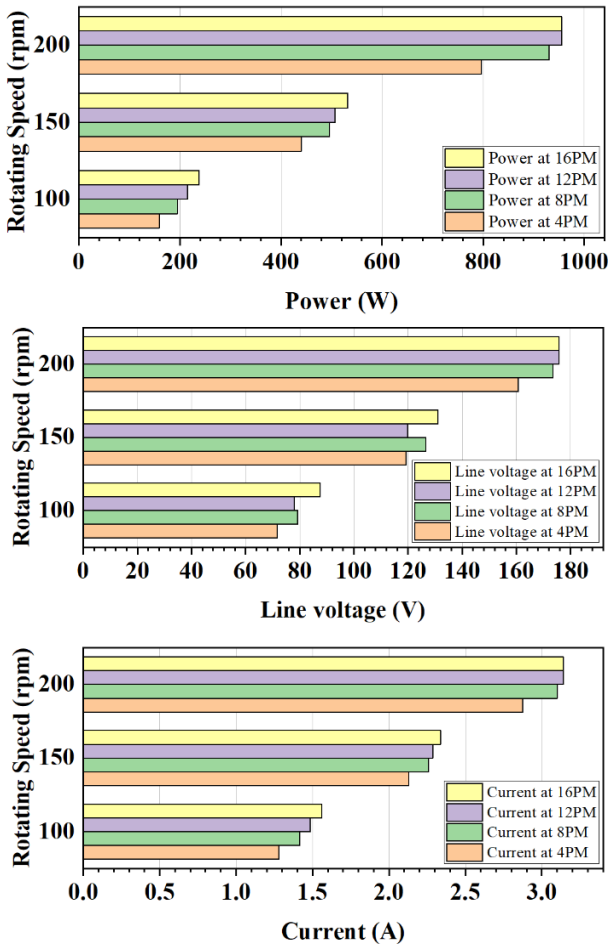

Fig. 13. Constant load analysis results of the 746 W HTSG at load resistance of 30 ohm.

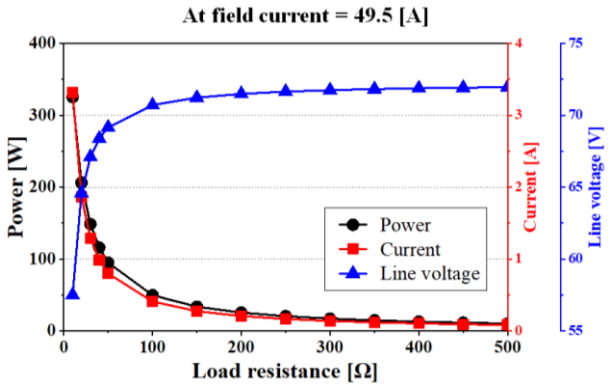

Fig. 14. Constant speed curves of 746 W HTSG at I_f of 49.5 A and N_s of 100 rpm.

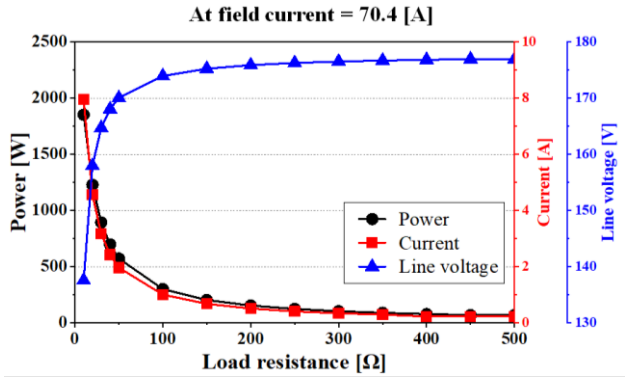

Fig. 15. Constant speed curves of 746 W HTSG at I_f of 70.4 A and N_s of 200 rpm.

4. CONCLUSION

In the preliminary charge tests, HTS field winding of the 746 W HTSG was successfully charged by 70 A class CSFE and its charge characteristics according to changes in the f_r. Moreover, 2-D electromagnetic FEA was performed based on I_f information in non-contact current charge tests to estimate the output characteristics of HTSG. It is positively possible to generate the rated output of 746 W using the I_f excitation of over 60 A with the f_r values of 13.3, 26.7, 40, and 53.3 Hz. All test and analysis results can be used as a technical reference for practical implementation and characteristic test of prototype HTSG equipped with 70 A class CSFE.

ACKNOWLEDGMENT

This work was supported in part by the National Research Foundation of Korea (NRF) grant funded by the Korea government (MSIT), Republic of Korea, and by Korea Electric Power Corporation. (Nos. 2019R1A2C1004715 and R18XA03)

REFERENCES

[1] C. Hoffmann, D. Pooke, and A. D. Caplin, "Flux pump for HTS magnets," *IEEE Trans. Appl. Supercond.*, vol. 21, no. 3, pp. 1628-1631, 2011.

[2] C. Hoffmann, R. Walsh, E. Karrer-Mueller, and D. Pooke, "Design parameters for an HTS flux pump," *Phys. Proc.*, vol. 36, pp. 1324-1329, 2012.

[3] R. M. Walsh, R. Slade, P. Donald, and C. Hoffmann, "Characterization of current stability in an HTS NMR system energized by an HTS flux pump," *IEEE Trans. Appl. Supercond.*, vol. 24, no. 3, Jun. 2014, Art. no. 4600805.

[4] Z. Jiang *et al.*, "A novel rotating HTS flux pump incorporating a ferromagnetic circuit," *IEEE Trans Appl. Supercond.*, vol. 26, no. 2, Mar. 2016, Art. no. 4900706.

[5] T. A. Coombs, J. F. Fagnard, and K. Matsuda, "Magnetization of 2-G coils and artificial bulks," *IEEE Trans. Appl. Supercond.*, vol. 24, no. 5, Oct. 2014, Art. no. 8201005.

[6] T. A. Coombs, J. Geng, L. Fu, and K. Matsuda, "An Overview of flux pumps for HTS Coils," *IEEE Trans Appl. Supercond.*, vol. 27, no. 4, Jun. 2017, Art. no. 4600806.

[7] C. W. Bumby, *et al.*, "Through-wall excitation of a magnet coil by an external-rotor HTS flux pump," *IEEE Trans Appl. Supercond.*, vol. 26, no. 3, Jun. 2016, Art. no. 0500505.

[8] C. W. Bumby *et al.*, "Development of a brushless HTS exciter for a 10 kW HTS synchronous generator," *Supercond. Sci. Technol.*, vol. 29, Jan. 2016, Art. no. 024008.

[9] V. Grinenko, G. Fuchs, J. Geng, and H. Zhang, "Dynamic resistance in a slab-like superconductor with J_c (B) dependence," *Supercond. Sci. Technol.*, vol. 12, pp. 382–387, 1999.

[10] J. Geng *et al.*, "Origin of dc voltage in type II superconducting flux pumps: Field, field rate of change, and current density dependence of resistivity," *J. Phys. D, Appl. Phys.*, vol. 49, no. 11, 2016, Art. no. 11LT01.

[11] Z. Jiang *et al.*, "Dynamic resistance of a high-Tc superconducting flux pump," *Appl. Phys. Lett.*, vol. 105, 2016, Art. no. 112601.

[12] C. W. Bumby, *et al.*, "Frequency dependent behavior of a dynamo-type HTS flux pump," *IEEE Trans Appl. Supercond.*, vol. 27, no. 4, Jun. 2017, Art. no. 5200705.

[13] Z. Jiang *et al.*, "Impact of flux gap upon dynamic resistance of a rotating HTS flux pump," *Supercond. Sci. Technol.*, vol. 28, Sep. 2015, Art. no. 115008.

[14] C. W. Bumby *et al.*, "Anomalous open-circuit voltage from a high-T_c superconducting dynamo," *Appl. Phys. Lett.*, vol. 108, no. 12, Mar. 2016. Art. no. 122601.

[15] R. C. Mataira *et al.*, "Origin of the DC output voltage from a high-T_c superconducting dynamo," *Appl. Phys. Lett.*, vol. 114, no. 16, Apr. 2019. Art. no. 162601.

[16] Z. Jiang *et al.*, "Dynamic resistance of a high-T_c superconducting flux pump," *Appl. Phys. Lett.*, vol. 105, Sept. 2014. Art. no. 112601.

[17] A. E. Pantoja *et al.*, "Impact of stator wire width on output of a dynamo-type HTS flux pump," *IEEE Trans. Appl. Supercond.*, vol. 26, no. 8, Dec. 2016, Art. no. 4805208.

[18] J. Lee *et al.*, "Experimental analysis of charging characteristics of HTS FCs with HTS contactless rotary excitation device considering various HTS loads," *IEEE Trans. Appl. Supercond.*, vol. 28, no. 3, Apr. 2018, Art. no. 5203105.

[19] H. Jeon *et al.*, "Methods for increasing the saturation current and charging speed of a rotary HTS flux-pump to charge the FC of a synchronous motor," *IEEE Trans. Appl. Supercond.*, vol. 28, no. 3, Apr. 2018, Art. no. 5202605.

[20] H. Jeon *et al.*, "PID control of an electromagnet-based rotary HTS flux pump for maintaining constant field in HTS synchronous motors," *IEEE Trans. Appl. Supercond.*, vol. 28, no. 4, Jun. 2018, Art. no. 5207605.

[21] S. Han *et al.*, "Charging characteristics of rotary HTS flux pump with several superconducting wires," *IEEE Trans. Appl. Supercond.*, vol. 29, no. 5, Aug. 2019, Art. no. 0603605.

[22] J. H. Kim *et al.*, "Design, analysis, and fabrication of salient field-pole for a 1-kW- HTS rotating machine," *Cryogenics*, vol. 97, pp. 126-132, 2019.

[23] J. H. Kim *et al.*, "Fabrication and charging test of HTS field windings using HTS contactless rotary excitation," *IEEE Trans. Appl. Supercond.*, vol. 29, no. 5, Aug. 2019, Art. no. 5203207.

[24] J. H. Kim *et al.*, "Fabrication and performance testing of a 1-kW-high-temperature superconducting generator with a high-temperature superconducting contactless field exciter," *Supercond. Sci. Technol.*, vol. 33, Jul. 2020, Art. no. 095003.

[25] C. J. Hyeon *et al.*, "Conceptual design of cooling anchor for current lead on HTS field coils," *Progr. Supercond. Cryogenics*, vol. 19, no. 2, pp. 38–43, 2017.

[26] T. D. Le *et al.*, "Conceptual design of current lead for large scale high temperature superconducting rotating machine," *Progr. Supercond. Cryogenics*, vol. 16, no. 2, pp. 54–58, 2014.

[27] Non-oriented electrical steel surface insulation, August. 22, 2017. [Online].Available:http://www.posco.co.kr/homepage/docs/eng5/dn/company/product/e_electrical_pdf_2011.pdf

[28] Lorenz J, Fowler JT. "Synchronous generator subtransient reactance prediction using transient circuit coupled electromagnetic analyses and odd periodic symmetry," August 22, 2017. [Online]. Available:http://studylib.net/doc/18175531/synchronous-generator-subtransient-reactance.